Sacrificial Cyclic Poly(phthalaldehyde) Templates for Low-Temperature Vascularization of Polymer Matrices

Article *in* ACS Applied Polymer Materials · December 2021

DOI: 10.1021/acsapm.1c01372

5 authors, including:

Xiang Zhang
University of Wyoming
22 PUBLICATIONS **141** CITATIONS

SEE PROFILE

Sacrificial Cyclic Poly(phthalaldehyde) Templates for Low-Temperature Vascularization of Polymer Matrices

Mayank Garg,[a,b] Adam C. Ladd,[a,b] Jia En Aw,[a,c] Xiang Zhang,[d] and Nancy R. Sottos[a,b]*

[a]Beckman Institute for Advanced Science and Technology, [b]Department of Materials Science and Engineering, [c]Department of Aerospace Engineering, University of Illinois at Urbana-Champaign, Urbana, Illinois, 61801

[d]Mechanical Engineering Department, University of Wyoming, Laramie, Wyoming, 82071

KEYWORDS

Cyclic poly(phthalaldehyde), thermal depolymerization, vascular, microchannel, wet-spinning, sacrificial polymer

ABSTRACT

Sacrificial polymers that depolymerize into small molecules upon exposure to an external stimulus facilitate the fabrication of synthetic structures with embedded vascular networks. Many sacrificial polymers such as poly(lactic acid) (PLA) and polycarbonates possess high thermal stability leading to a time- and energy-intensive vascularization process. Furthermore, use of these polymer templates is limited to high-temperature resistant (> 180 °C) matrices. Here, we demonstrate rapid vascularization of a range of host matrices through thermally triggered

depolymerization of cyclic poly(phthalaldehyde) (cPPA) at temperatures near 100 °C. Complete mass loss of solvent-cast cPPA films is observed within two hours at 100 °C in a thermogravimetric analyzer and after embedding in poly(dicyclopentadiene) matrices. Thermal processing of cPPA into sacrificial templates for inverse vascular architectures is hindered due to depolymerization at low temperatures. We successfully overcome these templating challenges by using solution spinning and 3D printing to fabricate fibers and printed templates, respectively. Microchannels are created inside low glass transition temperature (42 °C and 65 °C) epoxy-based matrices by depolymerizing the embedded fibers and printed templates within one hour at 110 °C. This low-temperature cPPA evacuation protocol enables vascularization of new matrices that would not survive the harsh thermal cycle required for depolymerizing existing sacrificial polymers. Moreover, cPPA depolymerization affords a five-fold reduction in the thermal energy consumed during template removal compared to PLA.

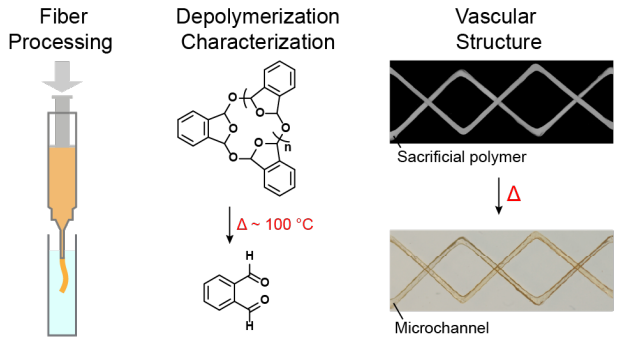

TOC figure

INTRODUCTION

Biological systems contain hierarchical vascular networks to mediate nutrient and fluid transport for repair, thermal regulation, and waste removal.[1] Incorporation of microchannels in synthetic matrices enables heat and mass transport in microfluidics,[2–8] microelectronics,[9–12] CO_2 sequestration,[13,14] flow batteries,[15] heat exchangers,[16] actively cooled structures,[17–22] and self-healing structures.[23–29] Several strategies have been adopted to create such microvascular structures including laser ablation,[5] dissolution,[3,4] lithography,[2,8,13] electrostatic discharge,[30] melting,[23,31–33] and template vaporization.[9,17,19,24,25,34] Catalyst-assisted thermal depolymerization of poly(lactic acid) (PLA) templates embedded in thermoset polymers and composites enables the fabrication of multifunctional vascular structures with versatile control over size and complexity of the microchannels.[24,25,27,34] This technique, termed as Vaporization of Sacrificial Components (VaSC), is energy-intensive (typically 200 °C for 12 hours), consuming 85 MJ of thermal energy for a one-meter long host structure.[35] Furthermore, VaSC of PLA templates is limited to host matrices that can sustain this thermal treatment without deformation or degradation. The depolymerization temperature decreases to 170 °C with more efficient catalysts and a reduction in the molecular weight of the templates, but the evacuation time increases considerably at lower temperatures.[27,36] Moreover, the catalyst particles remain on the microchannel surface after PLA depolymerization,[36,37] which may hinder subsequent functionalization of the vasculature. Sacrificial polymers that depolymerize at lower temperatures without catalysts are desirable for expanding vascularization to a broader range of host materials.[34]

In addition to rapid depolymerization at low temperatures, sacrificial polymers must be melt- or solution-processable into precise architectures and possess good mechanical properties to survive

thermomechanical loads during integration into the host matrix. Precision in channel dimensions becomes especially critical in microfluidic applications since the volumetric flow rate scales inversely with the fourth power of channel diameter. Depolymerization into gaseous products is preferred to enable complete evacuation of the high aspect ratio templates.[34] Compatibility between the matrix and the sacrificial polymer is also crucial since any physical or chemical interactions could inhibit the depolymerization and subsequent evaporation of the sacrificial templates.[11] Polymers that degrade in response to thermal, photo, and chemical stimuli are employed in recycling,[38–40] triggered release,[41–43] transient templates,[44–46] and signal amplification.[47–50] Unfortunately, most stimuli-responsive polymers do not have good mechanical properties for templating and integration into load-bearing host structures,[38,39,48] and require contact with liquid media for facilitating the degradation reaction.[40,42,48,51] Solvent access is limited to the exposed surfaces of the embedded templates in VaSC, making such stimuli-responsive polymers unsuitable for vascularization due to extremely slow diffusion-dominated degradation.[34]

Cyclic poly(phthalaldehyde) (cPPA) is a promising low ceiling temperature (-36 °C)[52] polymer that undergoes rapid unzipping from the solid state into monomers in response to mechanical, acidic, and thermal stimuli (**Scheme 1**).[53–60] Solution-processed cPPA capsules and films have been used for functional payload release[43] and transient substrates.[58,59,61] In this work, we investigate the processing and thermal depolymerization of sacrificial cPPA templates for creating microchannels in a variety of host matrices. cPPA is formed into films, fibers, and printed templates through solution-based methods, and its depolymerization kinetics are obtained experimentally and numerically. Evacuation of cPPA templates from several crosslinked

matrices is characterized at various temperatures and a low-temperature vascularization protocol is established for this new sacrificial polymer.

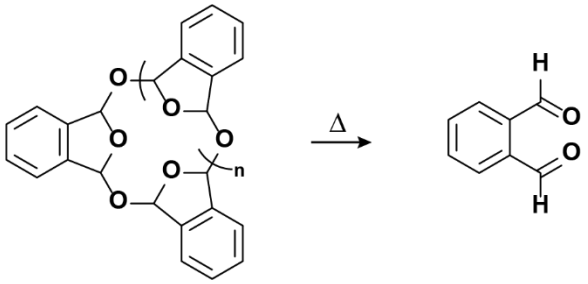

Scheme 1. Thermal depolymerization of cyclic poly(phthalaldehyde) (cPPA) to *o*PA monomer.

EXPERIMENTAL SECTION

Materials. High-performance liquid chromatography grade methanol, tetrahydrofuran (THF), and dichloromethane (DCM) were purchased from VWR. *ortho*-Phthalaldehyde (*o*PA) (99%) was procured from TCI America and purified by recrystallization as previously reported.[60] Dicyclopentadiene (DCPD), 2nd Generation Grubbs Catalyst (GC2), 5-ethylidene-2-norbornene (ENB), pentaerythritol tetrakis(3-mercaptopropionate) (tetrathiol), N,N-diglycidyl-4-glycidyoxyaniline (DGOA), (dimethylaminomethyl) phenol (catalyst 1) were purchased from Sigma Aldrich and used as received. Clear polydimethylsiloxane (PDMS) prepolymer (Sylgard 184) was purchased from DOW Corning. EPON 828 and EPIKURE 3233 were obtained from Hexion.

Solvent-casting of cPPA Films. Films were prepared using a modified procedure from the literature.[53–55,62] Synthesized cPPA (800 mg) was dissolved in DCM (5 mL) and vortexed for 30 min to ensure full dissolution. The solution was drop-cast into a Teflon-lined Petri dish with a diameter of 50 mm. The evaporation rate of DCM was slowed by placing another Petri dish

filled with DCM (10 mL) inside a film casting enclosure.[62] Slower evaporation was necessary to minimize surface defects and ensure uniform film thickness. The film was dried for 24 hours at room temperature (RT) in the saturated enclosure, followed by overnight drying under vacuum at 0.3 Torr. Film thickness (ca. 250 μm) was controlled by adjusting the initial amount of cPPA in the casting solution. The cPPA films were annealed at 90 °C for 15 min to reduce any residual stresses resulting from the casting process and stored at -20 °C until further use. The annealed films were cut into 20 mm x 5 mm rectangular strips using a 90 W CO_2 laser-cutter (Full Spectrum Laser, Pro Series). The strips were cleaned with isopropyl alcohol to remove any residual monomer on the edges due to laser ablation and weighed on an analytical balance (XPE205, Mettler-Toledo, ±0.03 mg) before embedding into various host matrices.

Wet-Spinning of cPPA Fibers. Synthesized cPPA was dissolved at 30 wt. % in different solvents and extruded inside a coagulation bath. Specifically, cPPA (1 g) was dissolved in THF (2.3 g) and vortexed overnight to create ca. 30% clear solution without any bubbles. A small amount of Nile Red dye was added to some solutions for visualization. The solution was transferred to a 5 mL glass syringe and mounted on a syringe pump (Legato 100, kd Scientific) followed by extrusion through a stainless-steel nozzle (Nordson EFD General Purpose Tips) submerged inside a measuring cylinder filled with methanol (1000 mL). Fibers with diameters ranging from 0.2 to 1.6 mm were made by varying nozzle gauges from 27 to 14. For example, a flow rate of 30 μL/min through a 22-gauge nozzle (internal diameter of 0.41 mm) yielded fibers with diameter ca. 0.4 mm. Fibers were kept submerged in methanol for ten minutes to complete the coagulation process and were subsequently dried overnight in a fume hood.

Solution-Printing of cPPA Templates. The printing ink (35% cPPA in THF) was prepared in a 3 mL syringe barrel (Optimum, Nordson EFD) and inserted into an HP3cc pneumatic dispensing

tool (Nordson EFD). The barrel was fitted with a 20-gauge stainless-steel nozzle (Optimum, Nordson EFD). A custom regulator controlled the air pressure to drive the ink extrusion process. The dispensing head was mounted on a robotic gantry (ABL9000, Aerotech Inc.) operated by a high-precision motion controller (A3200, Aerotech Inc.). A custom-designed software (RoboCAD 2.0) simultaneously controlled both the extrusion process and motion of the dispensing head. cPPA was extruded directly onto a glass plate submerged inside a methanol coagulation bath. The printed structures remained in the solvent bath for ten minutes and were subsequently removed and dried overnight in a fume hood.

Specimen Fabrication for Mass-Loss Experiments. Sacrificial film strips (20 mm x 5 mm x 250 μm) were embedded inside a poly(dicyclopentadiene) (pDCPD) matrix using a half-casting procedure. GC2 (0.52 mg) was dispersed in toluene (200 μL) and sonicated for five minutes. The catalyst solution was transferred to a scintillation vial containing 4 g of endo-DCPD mixed with 5 wt.% ENB. 0.13 mg of GC2 per 1 g of DCPD-ENB mixture was maintained for all resin formulations. Half of the DCPD resin (2 g) was poured into a 50 mm diameter aluminum dish and allowed to partially gel at RT for 120 minutes. Each laser-cut cPPA strip (20.0 ± 1.0 mg) was placed on the gelled DCPD surface with a cotton swab, then allowed to adhere for 30 minutes. Another 2 g of resin was added on top of the film and the matrix was subsequently cured at RT for 24 hours, followed by another 24 hours in a 35 °C oven. Each cured specimen containing an embedded sacrificial cPPA film was cut (16 mm x 8 mm x 2 mm) using a low-speed wet saw to expose the transverse ends of the film to the surroundings.

The mass of all samples was measured before placing them in a heated vacuum oven (Jeio Tech Co. Ltd., OV-11) for VaSC experiments. Each specimen was sandwiched between two aluminum plates to ensure uniform heating. The temperature of the oven was increased from RT

to the desired temperature under vacuum (0.5-1.0 Torr) and the isothermal temperature was held for 1-3 hours before cooling down to RT. The specimens were removed from the oven and their mass was measured to calculate the total mass loss after cPPA evacuation. The mass loss of neat pDCPD samples with similar dimensions as the VaSC specimens was also measured for each set of conditions (see **Supporting Information**).

VaSC of cPPA Fibers and Printed Templates in Crosslinked Matrices. Sacrificial fibers and printed structures were embedded in a pDCPD matrix using a cell casting procedure. The templates were clamped between two U-shaped rubber gaskets (each 1 mm thick) attached to two rectangular glass plates. The DCPD resin mixture (same formulation as above) was carefully poured into the glass mold to cover the sacrificial templates completely and cured according to the prior procedure. Solid samples were then removed from the mold and cut using a low-speed wet saw (50 mm x 8 mm x 2 mm) to expose the transverse ends of the sacrificial components before VaSC.

Sacrificial templates were embedded in a thiol-based epoxy matrix using the same cell-casting procedure as for the pDCPD samples. However, for these samples the glass plates were coated with a PTFE release agent (MS-122AD, Miller-Stephenson) before the templates were clamped. DGOA (7.5 g) was mixed with tetrathiol (9.9 g) at stoichiometry and stirred. Then catalyst 1 (174 mg) was added and the mixture was degassed at RT under 12 Torr vacuum for ten minutes (Yamato ADP31 drying oven, Welch 1402 pump). The resin-hardener mixture was poured into the glass mold containing the sacrificial elements and cured for 24 hours at RT. The specimens were cut with a low-speed wet saw to expose the transverse ends of the sacrificial templates for subsequent experiments. The procedures for cell-casting cPPA templates in amine-based epoxy and PDMS matrices are included in the **Supporting Information**.

Characterization. Mass loss of synthesized powder, films, and fibers (3 mg samples) in a nitrogen environment was measured on the TA Instruments thermogravimetric analyzer (TGA) Q500 system calibrated with nickel standards. For dynamic tests, the mass loss was recorded during a heating cycle over the temperature range from 40 °C to 250 °C at a linear ramp rate of 5 °C/min. For isothermal tests, the temperature was ramped from 40 °C to 10 °C below the desired temperature at a linear ramp rate of 10 °C/min, then subsequently ramped to the desired temperature at a linear ramp rate of 5 °C/min to minimize temperature overshoot. The isothermal temperature was maintained for three to six hours for each test.

Optical images of the pDCPD, epoxy, and PDMS samples before and after VaSC were obtained on a Keyence VHX-5000 digital microscope at 200x magnification.

Scanning electron micrographs (SEM) were acquired on an FEI Quanta FEG 450 ESEM. Samples were imaged at 5 kV after sputter coating with gold/palladium for 70 s using a Denton Desk II TSC-turbo-pumped sputter coater.

RESULTS AND DISCUSSION

Depolymerization of cPPA film templates. Drop-cast cPPA films were annealed and laser-cut into rectangular strips (**Figure 1a**). The mass loss of the cPPA films was monitored *ex situ* under dynamic and isothermal conditions using a thermogravimetric analyzer (TGA) (**Figure 2**). The depolymerization onset (T_d) of cPPA films (defined by 5% mass loss) was observed at 115 °C with complete mass loss at 140 °C in the dynamic TGA experiments at 5 °C/min (**Figure 2a**). In contrast, only 1% mass loss occurred for PLA films containing 3 wt. % tin (II) acetate in this temperature range.[36] Under isothermal conditions, significant mass loss of cPPA films occurred

only at temperatures greater than 85 °C (**Figure 2b**). As the exposure temperature increased from 90 °C to 110 °C, the time required for complete mass loss decreased from 3.5 hours to less than 1 hour. The PLA films containing 3% tin (II) acetate catalyst again showed negligible mass loss after 4 hours at 110 °C and complete vaporization was observed in eight hours at a much higher temperature of 200 °C (**Figure S1**).

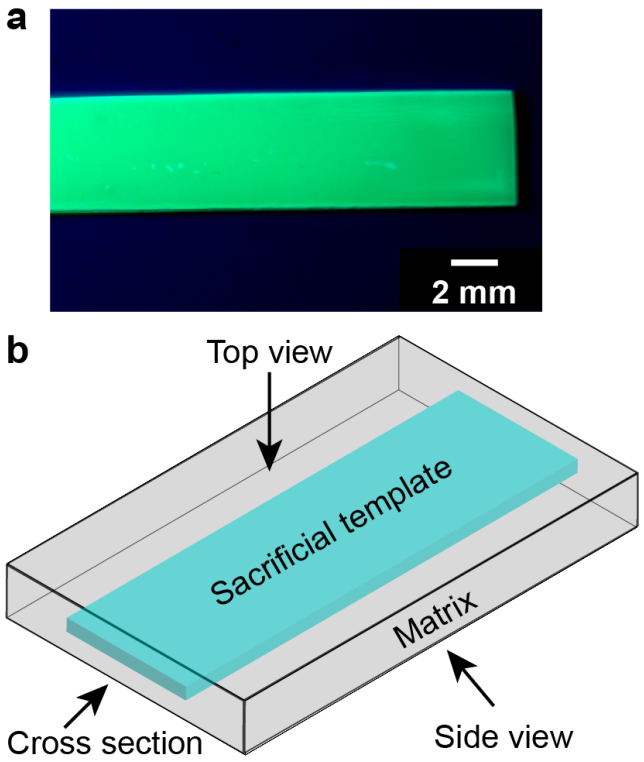

Figure 1. Specimen preparation for vascularization. (a) Optical image of ca. 250 µm thick cPPA film after laser cutting. The film was doped with trace amounts of fluorescent dye and imaged under UV light. (b) Schematic of a VaSC specimen showing a cPPA film embedded in a pDCPD matrix.

Next, the cPPA films were embedded in a pDCPD matrix, which will oxidize under the conditions required for vascularization with PLA templates (> 170 °C for 12 hours).[36] The transverse ends of templates (cross-sectional view in **Figure 1b**) were exposed to the

surrounding environment to facilitate the evacuation of gaseous monomer during the thermal cycle. Successful vascularization occurred with approximately 95% mass loss of the sacrificial template. Any small amount of residual monomer on the channel walls was easily flushed away with ethanol. Three hours of exposure at 90 °C resulted in blocked microchannels due to incomplete removal of cPPA with an average mass loss of 81% (**Figure 3a**), which is in qualitative agreement with the mass loss data for the films alone.

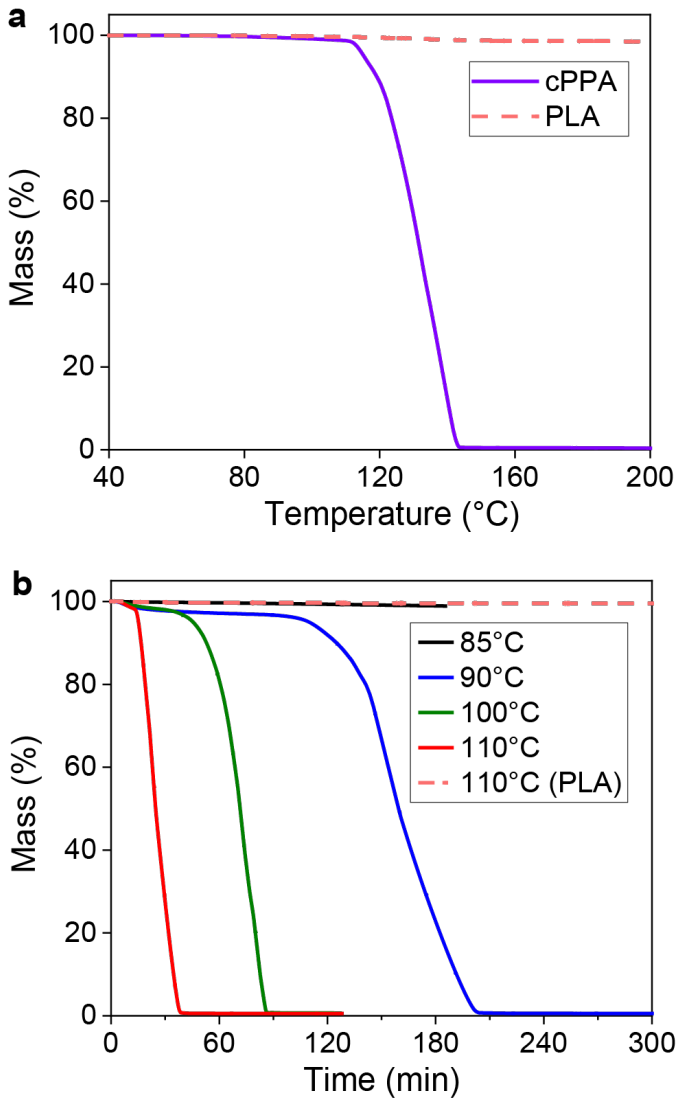

Figure 2. Mass loss of sacrificial polymer films under dynamic and isothermal conditions in a thermogravimetric analyzer (TGA). (a) Dynamic TGA data for cPPA and PLA films at 5 °C/min showing complete mass loss of cPPA between 100 and 140 °C. PLA films containing 3 wt. % tin

acetate catalyst[36] (dashed red line) did not show any mass loss in this temperature range. (b) Mass loss of cPPA films in isothermal TGA experiments. Mass loss of PLA containing 3% tin acetate[36] at 110 °C is indicated by the dashed red line.

Exposure for 3 hours at 100 °C led to successful vascularization with a mass loss of 98%. Optical (**Figure 3b-d**) and SEM (**Figure S3**) images of the pDCPD matrix post-VaSC showed residue-free microchannels with the same dimensions of the initial sacrificial cPPA templates. A dyed solution was injected into the microchannels to further confirm their clearance (**Figure 3c**). Specimens exposed to temperatures between 100-110 °C produced clear microchannels after a shorter duration of two hours. We were able to further reduce the exposure time to 1 hour through successful vascularization of specimens subjected to 105 °C and 110 °C, which is supported by the rapid mass loss of cPPA films at 110 °C in TGA experiments. These results show the high temperature-sensitivity of the cPPA mass loss kinetics. A marginal increase in exposure temperature from 90 to 100 °C allowed complete evacuation of cPPA templates after 2 hours, and the exposure time further reduced by 50% with a 5 °C increase in temperature to 105 °C. Thus, successful VaSC with cPPA is demonstrated at significantly lower temperatures than PLA, and the VaSC time is lowered below 1 hour with a modest increase in temperature.

The *in situ* VaSC characterization experiments show that cPPA enables rapid vascularization of host matrices at much lower temperatures than sacrificial PLA. Additionally, the resulting vasculature is residue-free following an ethanol rinse, providing the possibility for surface functionalization on the microchannel walls. However, solvent-cast films limit the overall dimensions, uniformity, and complexity of the sacrificial structures that can be fabricated[62] and hinder the creation of interconnected hollow networks. More advanced sacrificial cPPA architectures such as fibers and printed structures are required for creating multidimensional, interconnected vascular networks in various host matrices.

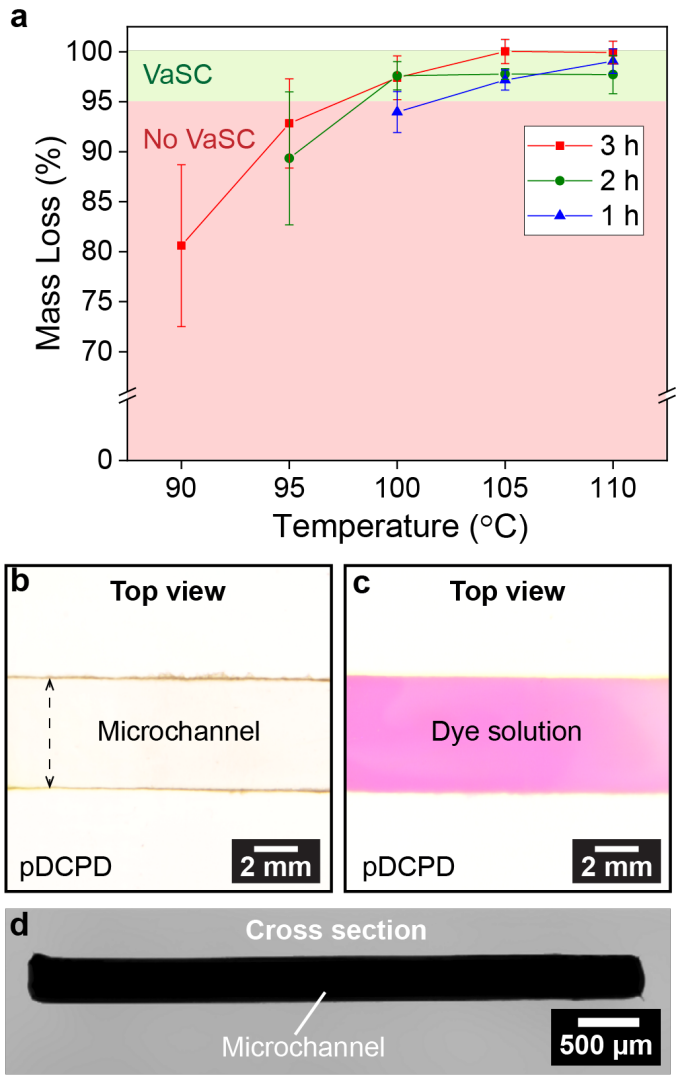

Figure 3. Thermal depolymerization characterization of cPPA films in vascularization experiments. (a) Mass loss of cPPA films embedded in pDCPD matrix after VaSC in a heated vacuum oven at various times and temperatures. Mass loss of 95% or higher was deemed sufficient for successful vascularization. Error bars represent one standard deviation (n = 6). Optical images showing the top view of the microchannel in pDCPD matrix created (b) after VaSC of cPPA film at 100 °C for three hours and (c) after infiltration with a dye solution (Nile Red in ethanol). (d) Cross section of the rectangular channel.

Vascularization with sacrificial fibers. Since cPPA depolymerizes before observable glass[54,60] or melt transition temperatures (**Figure S2**), solvent-based methods[63,64] are required for producing sacrificial fibers. We adopted a wet-spinning approach[64] to form cPPA fibers with a uniform cross section (**Figure 4a**). During wet-spinning, the polymer solution is extruded directly into a coagulation bath, allowing more control over the solvent removal process than dry-spinning. The difference in diffusion rates of the solvent exiting the fiber and counter-diffusion of non-solvent entering the fiber during coagulation plays a major role in dictating the cross-section of the freely extruded wet-spun fibers.[65] A slow coagulation process with roughly equal rates of diffusion and counter-diffusion results in a uniform fiber cross-section.[66] Several solvent and coagulant combinations were screened for controlling the fiber cross-section (see **Supporting Information**). Based on this screening, we selected tetrahydrofuran (THF) as the final solvent and methanol as the coagulant. A concentrated polymer solution (ca. 30 wt. % cPPA in solvent) was extruded into a methanol bath. The molecular weight of the starting cPPA was preserved after this wet-spinning step (**Table S1**), and fibers with a circular cross section and a smooth surface were obtained (**Figure 4b**). The final diameter of the fibers was tuned from 0.2 to 1.6 mm by changing the nozzle diameters during extrusion (**Figure 4c**).

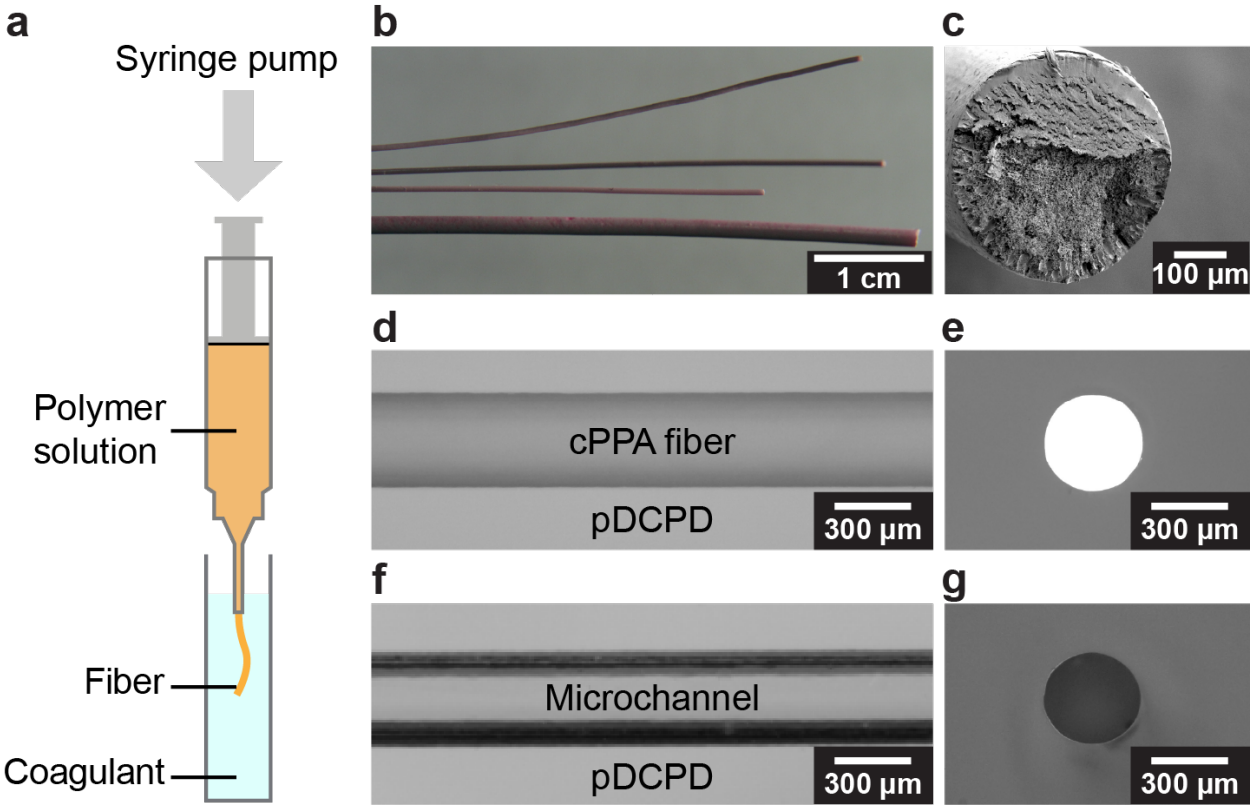

Figure 4. Vascularization of solution-processed cPPA fibers. (a) Schematic of the wet-spinning process in which a polymer solution containing 30 wt. % cPPA was extruded into a coagulation bath. (b) Optical micrographs of wet-spun cPPA fibers with diameters up to ca. 1.6 mm (containing Nile red dye) using tetrahydrofuran as the solvent and methanol as the coagulant. (c) Scanning electron microscopy (SEM) image of a cPPA fiber with a circular cross-section. Vascularization of pDCPD matrix with cPPA fibers. (d) Top and (e) cross-sectional view of a cPPA fiber embedded in pDCPD matrix before VaSC. (f) Top and (g) cross-sectional view of a microchannel in the matrix after VaSC at 110 °C for one hour.

These circular fibers were embedded in a pDCPD matrix and subsequently depolymerized at 110 °C for one hour (protocol established from previous mass-loss experiments) to obtain residue-free microchannels as shown in **Figure 4d-g**. X-ray computed microtomographic (µCT) reconstruction of the resulting microchannels confirmed that the channel dimensions matched well with the sacrificial precursor (**Figure S5**). cPPA fibers were embedded in three additional matrices with T_g < 100 °C (thiol-cured epoxy, amine-cured epoxy, and polydimethylsiloxane (PDMS)) to further demonstrate the advantages of low-temperature vascularization. Clear

microchannels after one hour at 110 °C were observed for the thiol- and amine-cured epoxy matrices with T_g ca. 42 °C and ca. 65 °C (**Figure S6**), respectively, without degradation of the host polymers (**Figure S7,8**). Fibers embedded in PDMS matrix with a T_g ca. -125 °C were also successfully evacuated under the same 110 °C / 1 h conditions (**Figure S9**). Increasing the temperature to 200 °C caused charring of the thiol-cured matrix (**Figure S10**) proving that sacrificial PLA is undesirable for vascularizing such matrices in short periods (< 3 h). Besides expanding vascularization to a broader range of matrices, cPPA allows substantial energy savings by cutting down the time and temperature required for the VaSC process. An estimation of the energy consumed in a 0.8 m^3 heated vacuum oven during vascularization shows a five-fold reduction for evacuating cPPA templates compared to PLA (**Table S3**).

Modeling depolymerization kinetics of cPPA. We developed a depolymerization kinetics model[67] to obtain the critical parameters that govern rapid depolymerization of cPPA at such low temperatures. An n^{th} order kinetic model that depends on the degree of cPPA depolymerization was used to simulate the mass loss behavior at different temperatures (**Equation 1**).

$$\frac{\partial \alpha}{\partial t} = A exp\left(-\frac{E}{RT}\right)(1-\alpha)^n \alpha^m \quad (1)$$

$$\alpha\,(t) = \frac{Intitial\ weight\ -\ Weight\ at\ time\ (t)}{Initial\ weight\ -\ Residual\ weight} \quad (2)$$

where, α (non-dimensional) denotes degree of depolymerization/conversion of cPPA; t (s) and T (K) denote time and temperature, respectively; E (kJ mol^{-1}), A (s^{-1}), and R (8.314 J mol^{-1} K^{-1}) denote the apparent activation energy, pre-exponential factor, and universal gas constant

respectively; n and m denote two constants associated with conversion that accounts for autocatalytic effects.

The mass loss of cPPA fibers was determined in TGA experiments and an optimization scheme provided the best-fit parameters for the depolymerization model in **Equation 1**. Since the T_d of a polymer is highly dependent on the heating rate,[68] the temporal derivative of the mass loss at three different ramp rates (**Figure 5a**) was used to capture the depolymerization kinetics in a broad range of temperatures. An apparent activation energy (E) of 89 kJ mol^{-1} and pre-exponential factor (A) of 4.4 x 10^9 s^{-1} accurately depict the mass loss behavior observed in dynamic TGA experiments. The 27% lower E for cPPA compared to 122 kJ mol^{-1} for PLA containing 3% tin acetate catalyst[36] (see **Table S2**) promotes its rapid depolymerization at significantly lower temperatures. The mass loss predictions are also in agreement with isothermal TGA experiments at three different temperatures (**Figure 5b**). Complete mass loss of cPPA fibers occurs in ca. 70 min at 100 °C, and increasing the temperature to 120 °C substantially reduces the depolymerization time to ca. 15 min. These findings suggests that the vascularization with cPPA templates can be achieved in a few minutes with a modest increase in temperature above 100 °C. Comparing the crucial modeling parameters that dictate the depolymerization kinetics of different sacrificial polymers would help establish vascularization protocols that are amenable to the thermal stability of the desired host matrix.

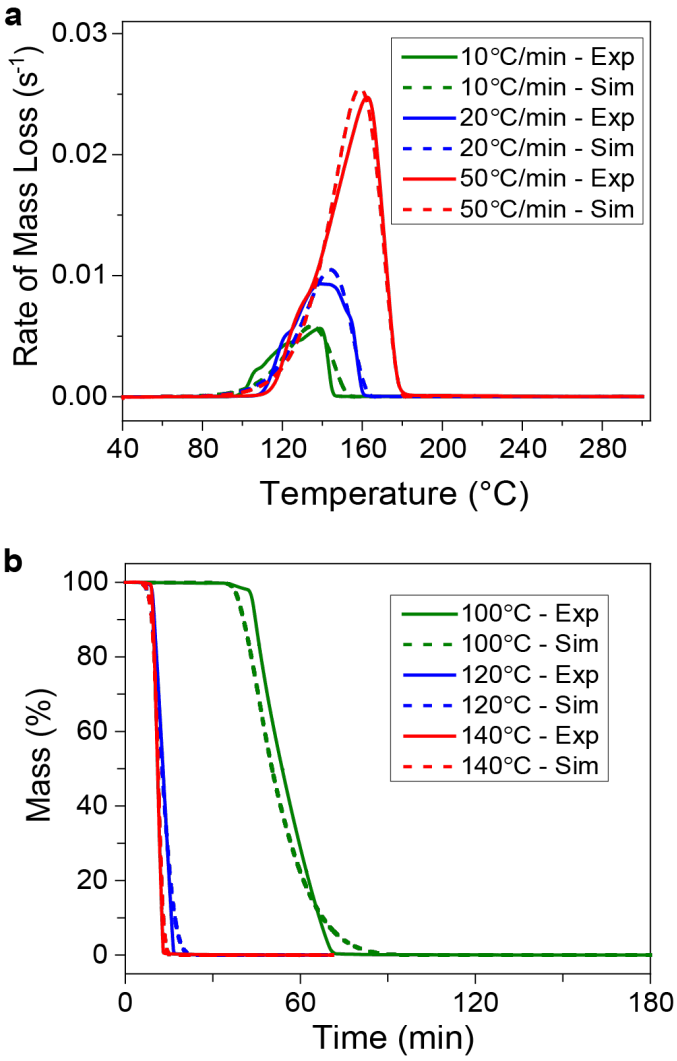

Figure 5. Comparison between TGA experiments (solid lines) and simulations (dashed lines) for mass loss of cPPA fibers. (a) Time derivative of mass loss at three ramp rates. (b) Mass remaining at three different isothermal temperatures. Model optimization was performed using MATLAB software.

Vascularization with printed cPPA templates. 3D printing of cPPA overcomes the templating challenges of solvent-cast films, achieve multi-dimensionality beyond 1D fibers, and provide a scalable approach with fine control over template dimensions. Precision in channel dimensions becomes especially critical in microfluidic applications since the volumetric flow rate scales inversely with the fourth power of channel diameter.[34] We used a direct ink writing technique,

resembling a wet-spinning process, to extrude cPPA solution (35% in THF) onto a glass slide submerged in a methanol bath (**Figure 6a**). The concentrated cPPA solution adheres to the glass slide upon extrusion and sets into the printed shape upon solvent diffusion. cPPA was printed in a zig-zag pattern for demonstration (**Figure 6b**). Two zig-zag templates were overlaid and embedded in a thiol-cured epoxy matrix. This specimen was vascularized at 110 °C for one hour, and the resulting microchannels were filled with dyed ethanol solution (**Figure 6c,d**). The two microchannels were interconnected at the overlapping regions where the sacrificial templates made physical contact before casting/evacuation. This fabrication strategy demonstrates a viable method for creating 2.5D/3D vasculatures by printing planar templates separately and stacking them before resin infusion. Realizing free-form 3D cPPA templates will require a viscoplastic coagulant which can mechanically support the print while also facilitating uniform diffusion of the solvent from the extruded solution.[69,70] A print bath with these desired features will allow the integration of complex sacrificial templates inside polymers and composites for manufacturing multifunctional vascular structures.

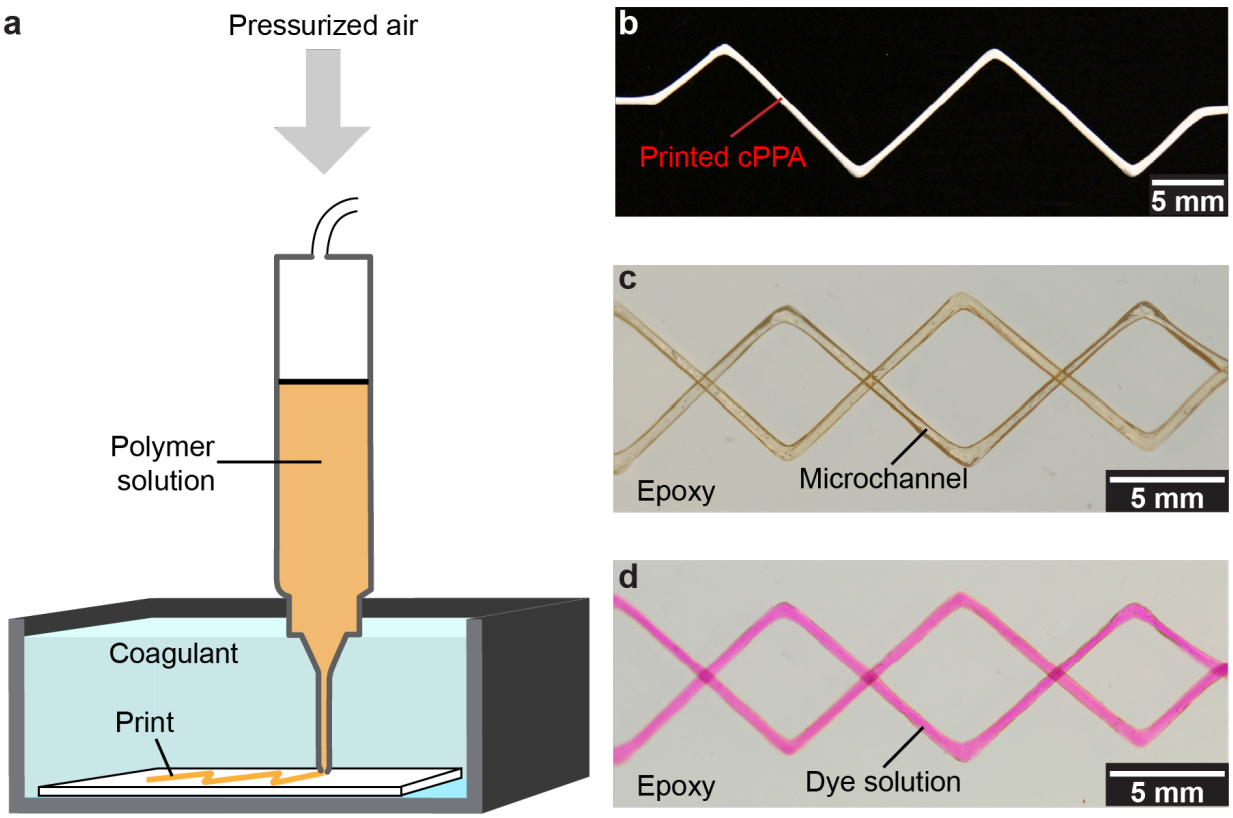

Figure 6. Printed cPPA templates for vascularization of a room temperature cured epoxy matrix. (a) Solvent-cast printing of a polymer solution containing a 35 wt.% cPPA into a coagulation bath. (b) Solvent-cast printed template using tetrahydrofuran (THF) as solvent and methanol as coagulant. (c) Top view of microchannels in the epoxy matrix after VaSC of two printed sacrificial templates at 110 °C for 1 hour. (d) Top view of the channel filled with a dye solution (Nile Red in ethanol) after VaSC.

CONCLUSIONS

In this work, we have created internal microvascular architectures through rapid depolymerization of cPPA templates resulting in a five-fold reduction in thermal energy consumption compared to existing sacrificial polymers. Transient cPPA templates with varied size scales and dimensionality were fabricated by employing different solvent-exchange methods on concentrated polymer solutions. The cross section and morphology of the transient templates were tuned by changing the diffusion rate of the solvent into the coagulation bath. Complete depolymerization and vaporization of cPPA templates without the need for additional catalysts

was observed after one hour at 110 °C in both *ex situ* TGA experiments, and *in situ* vascularization experiments with templates embedded in host matrices. Even though a narrow temperature range is explored for successful vascularization in this work, a further reduction is VaSC time is possible with slight increases in temperature, as suggested by TGA experiments and modeling. Optical, SEM, and micro-CT characterization confirmed that the microchannels were residue-free after an ethanol rinse. cPPA expands the scope of vascularization to matrices with low glass transition temperatures (< 150 °C), such as thiol- and amine-crosslinked epoxies cured at room temperature. We aim to extend this low-temperature VaSC technique via 3D printing to manufacture interconnected microvasculature in structural polymers and composites that resemble biological fluidic networks. This advancement hinges on obtaining mechanically robust templates that can survive the thermomechanical loads present during the fabrication of such host structures. The development of new processing routes to make complex cPPA templates may also find use in transient substrates for textiles and electronics applications.

ASSOCIATED CONTENT

Supporting Information. Pictures of cross-sections of cPPA fibers with different solvents, GPC on synthesized cPPA, DSC on synthesized cPPA, dynamic TGA on cPPA and PLA films, images of microchannels filled with ethanol solution containing Nile Red dye, images of cPPA fiber VaSC in thiol-cured epoxy, images of cPPA fiber VaSC in amine-cured epoxy, images of cPPA fiber VaSC in clear PDMS.

AUTHOR INFORMATION

Corresponding Author

*Email: n-sottos@illinois.edu

*ORCID ID:

Present Address

Materials Science and Engineering Building

1304 W. Green Street

Urbana, Illinois 61801

Funding Sources

Air Force Office of Scientific Research (AFOSR grant # FA9550-20-1-0194)

ACKNOWLEDGEMENTS

The authors acknowledge the funding and technical support from Air Force Office of Scientific Research (AFOSR grant # FA9550-20-1-0194, Center for Excellence in Self-healing to Morphogenic Manufacturing). Mayank Garg was also supported in part by a PPG-MRL Graduate Research Fellowship and Adam Ladd was supported by the Undergraduate Research Opportunity Program (UROP) from NASA's Illinois Space Grant Consortium. Xiang Zhang was supported by the faculty start-up funding provide by the University of Wyoming. The authors also acknowledge the Imaging Technology Group at the Beckman Institute for Advanced Science and Technology for SEM and EDAX equipment. The authors also extend their gratitude to Dr. Hector Lopez Hernandez (Stanford University), Prof. Mostafa Yourdkhani (Colorado State University), Prof. Scott R. White (University of Illinois) for helpful discussions.

REFERENCES

(1) Campbell, N. A.; Reece, J. B.; Taylor, M. R.; Simon, E. J.; Dickey, J. L. *Biology*; Benjamin Cummings; Benjamin Cummings, 2010.

(2) Unger, M. A.; Chou, H.-P.; Thorsen, T.; Scherer, A.; Quake, S. R. Monolithic Microfabricated Valves and Pumps by Multilayer Soft Lithography. *Science* **2000**, *288* (5463), 113–116. https://doi.org/10.1126/science.288.5463.113.

(3) Bellan, L. M.; Singh, S. P.; Henderson, P. W.; Porri, T. J.; Craighead, H. G.; Spector, J. A. Fabrication of an Artificial 3-Dimensional Vascular Network Using Sacrificial Sugar Structures. *Soft Matter* **2009**, *5* (7), 1354–1357. https://doi.org/10.1039/b819905a.

(4) Gualandi, C.; Zucchelli, A.; Osorio, M. F.; Belcari, J.; Focarete, M. L. Nanovascularization of Polymer Matrix: Generation of Nanochannels and Nanotubes by Sacrificial Electrospun Fibers. *Nano Lett* **2013**, *13* (11), 5385–5390. https://doi.org/10.1021/nl402930x.

(5) Lim, D.; Kamotani, Y.; Cho, B.; Mazumder, J.; Takayama, S. Fabrication of Microfluidic Mixers and Artificial Vasculatures Using a High-Brightness Diode-Pumped Nd:YAG Laser Direct Write Method. *Lab on a chip* **2003**, *3* (4), 318–323. https://doi.org/10.1039/b308452c.

(6) Zhou, Y. The Recent Development and Applications of Fluidic Channels by 3D Printing. *J Biomed Sci* **2017**, *24* (1), 80. https://doi.org/10.1186/s12929-017-0384-2.

(7) Wu, W.; DeConinck, A.; Lewis, J. A. Omnidirectional Printing of 3D Microvascular Networks. *Adv. Mater.* **2011**, *23* (24), H178–H183. https://doi.org/10.1002/adma.201004625.

(8) Colosi, C.; Shin, S. R.; Manoharan, V.; Massa, S.; Costantini, M.; Barbetta, A.; Dokmeci, M. R.; Dentini, M.; Khademhosseini, A. Microfluidic Bioprinting of Heterogeneous 3D Tissue Constructs Using Low-Viscosity Bioink. *Adv Mater* **2015**, *28* (4), 677–684. https://doi.org/10.1002/adma.201503310.

(9) Jayachandran, J. P.; Reed, H. A.; Zhen, H.; Rhodes, L. F.; Henderson, C. L.; Allen, S. A. B.; Kohl, P. A. Air-Channel Fabrication for Microelectromechanical Systems via Sacrificial Photosensitive Polycarbonates. *Journal of Microelectromechanical Systems* **2003**, *12* (2), 147–159. https://doi.org/10.1109/jmems.2003.809963.

(10) Joseph, P. J.; Monajemi, P.; Ayazi, F.; Kohl, P. A. Wafer-Level Packaging of Micromechanical Resonators. *IEEE Transactions on Advanced Packaging* **2007**, *30* (1), 19–26. https://doi.org/10.1109/tadvp.2006.890220.

(11) Spencer, T. J.; Chen, Y.-C.; Saha, R.; Kohl, P. A. Stabilization of the Thermal Decomposition of Poly(Propylene Carbonate) Through Copper Ion Incorporation and Use in

Self-Patterning. *Journal of Electronic Materials* **2011**, *40* (6), 1350–1363. https://doi.org/10.1007/s11664-011-1518-z.

(12) Uzunlar, E.; Kohl, P. A. Size-Compatible, Polymer-Based Air-Gap Formation Processes, and Polymer Residue Analysis for Wafer-Level MEMS Packaging Applications. *Journal of Electronic Packaging* **2015**, *137* (4), 041001–041013. https://doi.org/10.1115/1.4030952.

(13) Potkay, J. A.; Magnetta, M.; Vinson, A.; Cmolik, B. Bio-Inspired, Efficient, Artificial Lung Employing Air as the Ventilating Gas. *Lab Chip* **2011**, *11* (17), 2901–2909. https://doi.org/10.1039/c1lc20020h.

(14) Nguyen, D. T.; Leho, Y. T.; Esser-Kahn, A. P. A Three-Dimensional Microvascular Gas Exchange Unit for Carbon Dioxide Capture. *Lab Chip* **2012**, *12* (7), 1246–1250. https://doi.org/10.1039/c2lc00033d.

(15) Weber, A. Z.; Mench, M. M.; Meyers, J. P.; Ross, P. N.; Gostick, J. T.; Liu, Q. Redox Flow Batteries: A Review. *J. Appl. Electrochem.* **2011**, *41* (10), 1137–1164. https://doi.org/10.1007/s10800-011-0348-2.

(16) Maloney, K. J.; Fink, K. D.; Schaedler, T. A.; Kolodziejska, J. A.; Jacobsen, A. J.; Roper, C. S. Multifunctional Heat Exchangers Derived from Three-Dimensional Micro-Lattice Structures. *Int. J. Heat Mass Transf.* **2012**, *55* (9–10), 2486–2493. https://doi.org/10.1016/j.ijheatmasstransfer.2012.01.011.

(17) Pety, S. J.; Chia, P. X. L.; Carrington, S. M.; White, S. R. Active Cooling of Microvascular Composites for Battery Packaging. *Smart Mater Struct* **2017**, *26* (10), 105004. https://doi.org/10.1088/1361-665x/aa84e7.

(18) Coppola, A. M.; Hu, L.; Thakre, P. R.; Radovic, M.; Karaman, I.; Sottos, N. R.; White, S. R. Active Cooling of a Microvascular Shape Memory Alloy-Polymer Matrix Composite Hybrid Material . *Adv Eng Mater* **2016**, *18* (7), 1145–1153. https://doi.org/10.1002/adem.201600020.

(19) Coppola, A. M.; Warpinski, L. G.; Murray, S. P.; Sottos, N. R.; White, S. R. Survival of Actively Cooled Microvascular Polymer Matrix Composites under Sustained Thermomechanical Loading. *Compos Part Appl Sci Manuf* **2016**, *82*, 170–179. https://doi.org/10.1016/j.compositesa.2015.12.010.

(20) Pety, S. J.; Tan, M. H. Y.; Najafi, A. R.; Barnett, P. R.; Geubelle, P. H.; White, S. R. Carbon Fiber Composites with 2D Microvascular Networks for Battery Cooling. *Int. J. Heat Mass Transf.* **2017**, *115*, 513–522. https://doi.org/10.1016/j.ijheatmasstransfer.2017.07.047.

(21) Pety, S. J.; Tan, M. H. Y.; Najafi, A. R.; Gendusa, A. C.; Barnett, P. R.; Geubelle, P. H.; White, S. R. Design of Redundant Microvascular Cooling Networks for Blockage Tolerance. *Appl Therm Eng* **2018**, *131* (Int. J. Heat Mass Transf. 103 2016), 965–976. https://doi.org/10.1016/j.applthermaleng.2017.10.094.

(22) Pejman, R.; Aboubakr, S. H.; Martin, W. H.; Devi, U.; Tan, M. H. Y.; Patrick, J. F.; Najafi, A. R. Gradient-Based Hybrid Topology/Shape Optimization of Bioinspired Microvascular Composites. *Int J Heat Mass Tran* **2019**, *144*, 118606. https://doi.org/10.1016/j.ijheatmasstransfer.2019.118606.

(23) Toohey, K. S.; Sottos, N. R.; Lewis, J. A.; Moore, J. S.; White, S. R. Self-Healing Materials with Microvascular Networks. *Nat. Mater.* **2007**, *6* (8), 581–585. https://doi.org/10.1038/nmat1934.

(24) Esser-Kahn, A. P.; Thakre, P. R.; Dong, H.; Patrick, J. F.; Vlasko-Vlasov, V. K.; Sottos, N. R.; Moore, J. S.; White, S. R. Three-Dimensional Microvascular Fiber-Reinforced Composites. *Adv. Mater.* **2011**, *23* (32), 3654–3658. https://doi.org/10.1002/adma.201100933.

(25) Patrick, J. F.; Hart, K. R.; Krull, B. P.; Diesendruck, C. E.; Moore, J. S.; White, S. R.; Sottos, N. R. Continuous Self-Healing Life Cycle in Vascularized Structural Composites. *Adv. Mater.* **2014**, *26* (25), 4302–4308. https://doi.org/10.1002/adma.201400248.

(26) Hart, K. R.; Lankford, S. M.; Freund, I. A.; Patrick, J. F.; Krull, B. P.; Wetzel, E. D.; Sottos, N. R.; White, S. R. Repeated Healing of Delamination Damage in Vascular Composites by Pressurized Delivery of Reactive Agents. *Composites Science and Technology* **2017**, *151*, 1–9. https://doi.org/10.1016/j.compscitech.2017.07.027.

(27) Patrick, J. F.; Krull, B. P.; Garg, M.; Mangun, C. L.; Moore, J. S.; Sottos, N. R.; White, S. R. Robust Sacrificial Polymer Templates for 3D Interconnected Microvasculature in Fiber-Reinforced Composites. *Compos. Part A Appl. Sci. Manuf.* **2017**, *100*, 361–370. https://doi.org/10.1016/j.compositesa.2017.05.022.

(28) Norris, C. J.; White, J. A. P.; McCombe, G.; Chatterjee, P.; Bond, I. P.; Trask, R. S. Autonomous Stimulus Triggered Self-Healing in Smart Structural Composites. *Smart Materials and Structures* **2012**, *21* (9), 094027. https://doi.org/10.1088/0964-1726/21/9/094027.

(29) Dean, L. M.; Krull, B. P.; Li, K. R.; Fedonina, Y. I.; White, S. R.; Sottos, N. R. Enhanced Mixing of Microvascular Self-Healing Reagents Using Segmented Gas–Liquid Flow. *Acs Appl Mater Inter* **2018**, *10* (38), 32659–32667. https://doi.org/10.1021/acsami.8b09966.

(30) Huang, J.-H.; Kim, J.; Agrawal, N.; Sudarsan, A. P.; Maxim, J. E.; Jayaraman, A.; Ugaz, V. M. Rapid Fabrication of Bio-Inspired 3D Microfluidic Vascular Networks. *Advanced Materials* **2009**, *21* (35), 3567–3571. https://doi.org/10.1002/adma.200900584.

(31) Therriault, D.; White, S. R.; Lewis, J. A. Chaotic Mixing in Three-Dimensional Microvascular Networks Fabricated by Direct-Write Assembly. *Nat. Mater.* **2003**, *2* (4), 265–271. https://doi.org/10.1038/nmat863.

(32) Norris, C. J.; Bond, I. P.; Trask, R. S. Interactions between Propagating Cracks and Bioinspired Self-Healing Vascules Embedded in Glass Fibre Reinforced Composites. *Compos. Sci. Technol.* **2011**, *71* (6), 847–853. https://doi.org/10.1016/j.compscitech.2011.01.027.

(33) Hansen, C. J.; Wu, W.; Toohey, K. S.; Sottos, N. R.; White, S. R.; Lewis, J. A. Self-Healing Materials with Interpenetrating Microvascular Networks. *Advanced Materials* **2009**, *21* (41), 4143–4147. https://doi.org/10.1002/adma.200900588.

(34) Gergely, R. C. R.; Pety, S. J.; Krull, B. P.; Patrick, J. F.; Doan, T. Q.; Coppola, A. M.; Thakre, P. R.; Sottos, N. R.; Moore, J. S.; White, S. R. Multidimensional Vascularized Polymers Using Degradable Sacrificial Templates. *Adv. Funct. Mater.* **2014**, *25* (7), 1043–1052. https://doi.org/10.1002/adfm.201403670.

(35) Witik, R. A.; Gaille, F.; Teuscher, R.; Ringwald, H.; Michaud, V.; Månson, J.-A. E. Economic and Environmental Assessment of Alternative Production Methods for Composite Aircraft Components. *J. Clean. Prod.* **2012**, *29*, 91–102. https://doi.org/10.1016/j.jclepro.2012.02.028.

(36) Garg, M.; White, S. R.; Sottos, N. R. Rapid Degradation of Poly(Lactic Acid) with Organometallic Catalysts. *Acs Appl Mater Inter* **2019**, *11* (49), 46226–46232. https://doi.org/10.1021/acsami.9b17599.

(37) Dong, H.; Esser-Kahn, A. P.; Thakre, P. R.; Patrick, J. F.; Sottos, N. R.; White, S. R.; Moore, J. S. Chemical Treatment of Poly(Lactic Acid) Fibers to Enhance the Rate of Thermal Depolymerization. *ACS Applied Materials & Interfaces* **2012**, *4* (2), 503–509. https://doi.org/10.1021/am2010042.

(38) Baker, M. S.; Kim, H.; Olah, M. G.; Lewis, G. G.; Phillips, S. T. Depolymerizable Poly(Benzyl Ether)-Based Materials for Selective Room Temperature Recycling. *Green Chemistry* **2015**, *17* (9), 4541–4545. https://doi.org/10.1039/c5gc01090j.

(39) Fan, B.; Trant, J. F.; Yardley, R. E.; Pickering, A. J.; Lagugné-Labarthet, F.; Gillies, E. R. Photocontrolled Degradation of Stimuli-Responsive Poly(Ethyl Glyoxylate): Differentiating Features and Traceless Ambient Depolymerization. *Macromolecules* **2016**, *49* (19), 7196–7203. https://doi.org/10.1021/acs.macromol.6b01620.

(40) Zhu, J.-B.; Watson, E. M.; Tang, J.; Chen, E. Y. X. A Synthetic Polymer System with Repeatable Chemical Recyclability. *Science* **2018**, *360* (6387), 398–403. https://doi.org/10.1126/science.aar5498.

(41) Dilauro, A. M.; Abbaspourrad, A.; Weitz, D. A.; Phillips, S. T. Stimuli-Responsive Core–Shell Microcapsules with Tunable Rates of Release by Using a Depolymerizable Poly(Phthalaldehyde) Membrane. *Macromolecules* **2013**, *46* (9), 3309–3313. https://doi.org/10.1021/ma400456p.

(42) Zhang, Y.; Ma, L.; Deng, X.; Cheng, J. Trigger-Responsive Chain-Shattering Polymers. *Polymer Chemistry* **2013**, *4* (2), 224–228. https://doi.org/10.1039/c2py20838e.

(43) Tang, S.; Yourdkhani, M.; Casey, C. M. P.; Sottos, N. R.; White, S. R.; Moore, J. S. Low-Ceiling-Temperature Polymer Microcapsules with Hydrophobic Payloads via Rapid Emulsion-

Solvent Evaporation. *ACS Applied Materials & Interfaces* **2017**, *9* (23), 20115–20123. https://doi.org/10.1021/acsami.7b05266.

(44) Uzunlar, E.; Schwartz, J.; Phillips, O.; Kohl, P. A. Decomposable and Template Polymers: Fundamentals and Applications. *J. Electron. Packag.* **2016**, *138* (2), 020802–020815. https://doi.org/10.1115/1.4033000.

(45) Ohlendorf, P.; Ruyack, A.; Leonardi, A.; Shi, C.; Cuppoletti, C.; Bruce, I.; Lal, A.; Ober, C. K. Transient Fiber Mats of Electrospun Poly(Propylene Carbonate) Composites with Remarkable Mechanical Strength. *ACS Applied Materials & Interfaces* **2017**, *9* (30), 25495–25505. https://doi.org/10.1021/acsami.7b04710.

(46) Camera, K. L.; Wenning, B.; Lal, A.; Ober, C. K. Transient Materials from Thermally-Sensitive Polycarbonates and Polycarbonate Nanocomposites. *Polymer* **2016**, *101*, 59–66. https://doi.org/10.1016/j.polymer.2016.08.050.

(47) Phillips, S. T.; Robbins, J. S.; DiLauro, A. M.; Olah, M. G. Amplified Responses in Materials Using Linear Polymers That Depolymerize from End-to-End When Exposed to Specific Stimuli. *J Appl Polym Sci* **2014**, *131* (19), n/a-n/a. https://doi.org/10.1002/app.40992.

(48) Sagi, A.; Weinstain, R.; Karton, N.; Shabat, D. Self-Immolative Polymers. *Journal of the American Chemical Society* **2008**, *130* (16), 5434–5435. https://doi.org/10.1021/ja801065d.

(49) DiLauro, A. M.; Phillips, S. T. End-Capped Poly(4,5-Dichlorophthalaldehyde): A Stable Self-Immolative Poly(Aldehyde) for Translating Specific Inputs into Amplified Outputs, Both in Solution and the Solid State. *Polym Chem-uk* **2015**, *6* (17), 3252–3258. https://doi.org/10.1039/c5py00190k.

(50) Lewis, G. G.; Robbins, J. S.; Phillips, S. T. A Prototype Point-of-Use Assay for Measuring Heavy Metal Contamination in Water Using Time as a Quantitative Readout. *Chemical Communications* **2014**, *50* (40), 5352–5354. https://doi.org/10.1039/c3cc47698g.

(51) Peterson, G. I.; Larsen, M. B.; Boydston, A. J. Controlled Depolymerization: Stimuli-Responsive Self-Immolative Polymers. **2012**, *45* (18), 7317–7328. https://doi.org/10.1021/ma300817v.

(52) Lutz, J. P.; Davydovich, O.; Hannigan, M. D.; Moore, J. S.; Zimmerman, P. M.; McNeil, A. J. Functionalized and Degradable Polyphthalaldehyde Derivatives. *J Am Chem Soc* **2019**, *141* (37), 14544–14548. https://doi.org/10.1021/jacs.9b07508.

(53) Feinberg, E. C.; Davydovich, O.; Lloyd, E. M.; Ivanoff, D. G.; Shiang, B.; Sottos, N. R.; Moore, J. S. Triggered Transience of Plastic Materials by a Single Electron Transfer Mechanism. *Acs Central Sci* **2020**, *6* (2), 266–273. https://doi.org/10.1021/acscentsci.9b01237.

(54) Lloyd, E. M.; Hernandez, H. L.; Feinberg, E. C.; Yourdkhani, M.; Zen, E. K.; Mejia, E. B.; Sottos, N. R.; Moore, J. S.; White, S. R. Fully Recyclable Metastable Polymers and Composites. *Chem Mater* **2018**, *31* (2), 398–406. https://doi.org/10.1021/acs.chemmater.8b03585.

(55) Feinberg, E. C.; Hernandez, H. L.; Plantz, C. L.; Mejia, E. B.; Sottos, N. R.; White, S. R.; Moore, J. S. Cyclic Poly(Phthalaldehyde): Thermoforming a Bulk Transient Material. *Acs Macro Lett* **2018**, *7* (1), 47–52. https://doi.org/10.1021/acsmacrolett.7b00769.

(56) Hernandez, H. L.; Lee, O. P.; Casey, C. M. P.; Kaitz, J. A.; Park, C. W.; Plantz, C. L.; Moore, J. S.; White, S. R. Accelerated Thermal Depolymerization of Cyclic Polyphthalaldehyde with a Polymeric Thermoacid Generator. *Macromol Rapid Comm* **2018**, *39* (11), 1800046. https://doi.org/10.1002/marc.201800046.

(57) Diesendruck, C. E.; Peterson, G. I.; Kulik, H. J.; Kaitz, J. A.; Mar, B. D.; May, P. A.; White, S. R.; Martínez, T. J.; Boydston, A. J.; Moore, J. S. Mechanically Triggered Heterolytic Unzipping of a Low-Ceiling-Temperature Polymer. *Nature Chemistry* **2014**, *6* (7), 623–628. https://doi.org/10.1038/nchem.1938.

(58) Hernandez, H. L.; Kang, S.-K.; Lee, O. P.; Hwang, S.-W.; Kaitz, J. A.; Inci, B.; Park, C. W.; Chung, S.; Sottos, N. R.; Moore, J. S.; Rogers, J. A.; White, S. R. Triggered Transience of Metastable Poly(Phthalaldehyde) for Transient Electronics. *Advanced Materials* **2014**, *26* (45), 7637–7642. https://doi.org/10.1002/adma.201403045.

(59) Park, C. W.; Kang, S.-K.; Hernandez, H. L.; Kaitz, J. A.; Wie, D. S.; Shin, J.; Lee, O. P.; Sottos, N. R.; Moore, J. S.; Rogers, J. A.; White, S. R. Thermally Triggered Degradation of Transient Electronic Devices. *Advanced Materials* **2015**, *27* (25), 3783–3788. https://doi.org/10.1002/adma.201501180.

(60) Kaitz, J. A.; Diesendruck, C. E.; Moore, J. S. End Group Characterization of Poly(Phthalaldehyde): Surprising Discovery of a Reversible, Cationic Macrocyclization Mechanism. *Journal of the American Chemical Society* **2013**, *135* (34), 12755–12761. https://doi.org/10.1021/ja405628g.

(61) Lee, K. M.; Phillips, O.; Engler, A.; Kohl, P. A.; Rand, B. P. Phototriggered Depolymerization of Flexible Poly(Phthalaldehyde) Substrates by Integrated Organic Light-Emitting Diodes. *Acs Appl Mater Inter* **2018**, *10* (33), 28062–28068. https://doi.org/10.1021/acsami.8b08181.

(62) Hernandez, H. L.; Takekuma, S. K.; Mejia, E. B.; Plantz, C. L.; Sottos, N. R.; Moore, J. S.; White, S. R. Processing-Dependent Mechanical Properties of Solvent Cast Cyclic Polyphthalaldehyde. *Polymer* **2019**, *162* (J. Am. Chem. Soc. 135 2013), 29–34. https://doi.org/10.1016/j.polymer.2018.12.016.

(63) Imura, Y.; Hogan, R. M. C.; Jaffe, M. 10 Dry Spinning of Synthetic Polymer Fibers; Advances in Filament Yarn Spinning of Textiles and Polymers; Elsevier, 2014; pp 187–202. https://doi.org/10.1533/9780857099174.2.187.

(64) Ozipek, B.; Karakas, H. Wet Spinning of Synthetic Polymer Fibers; Advances in Filament Yarn Spinning of Textiles and Polymers; Elsevier, 2014; pp 174–186. https://doi.org/10.1533/9780857099174.2.174.

(65) Wang, Y.-X.; Wang, C.-G.; Bai, Y.-J.; Bo, Z. Effect of the Drawing Process on the Wet Spinning of Polyacrylonitrile Fibers in a System of Dimethyl Sulfoxide and Water. *Journal of Applied Polymer Science* **2007**, *104* (2), 1026–1037. https://doi.org/10.1002/app.24793.

(66) Wei, H.; Suo, X.; Lu, C.; Liu, Y. A Comparison of Coagulation and Gelation on the Structures and Stabilization Behaviors of Polyacrylonitrile Fibers. *J Appl Polym Sci* **2019**, *137* (19), 48671. https://doi.org/10.1002/app.48671.

(67) Das, P.; Tiwari, P. Thermal Degradation Kinetics of Plastics and Model Selection. *Thermochimica Acta* **2017**, *654*, 191–202. https://doi.org/10.1016/j.tca.2017.06.001.

(68) Spencer, T. J.; Kohl, P. A. Decomposition of Poly(Propylene Carbonate) with UV Sensitive Iodonium Salts. *Polym. Degrad. Stab.* **2011**, *96* (4), 686–702. https://doi.org/10.1016/j.polymdegradstab.2010.12.003.

(69) Muth, J. T.; Vogt, D. M.; Truby, R. L.; Mengüç, Y.; Kolesky, D. B.; Wood, R. J.; Lewis, J. A. Embedded 3D Printing of Strain Sensors within Highly Stretchable Elastomers. *Adv Mater* **2014**, *26* (36), 6307–6312. https://doi.org/10.1002/adma.201400334.

(70) Grosskopf, A. K.; Truby, R. L.; Kim, H.; Perazzo, A.; Lewis, J. A.; Stone, H. A. Viscoplastic Matrix Materials for Embedded 3D Printing. *Acs Appl Mater Inter* **2018**, *10* (27), 23353–23361. https://doi.org/10.1021/acsami.7b19818.